Electronic Supplementary Material (ESI) for ChemComm.

Supplementary Information

Selective Methane Photooxidation into Methanol under Mild Conditions Promoted by Highly Dispersed Cu Atoms on Crystalline Carbon Nitrides

Marcos A. R. Silva,[a,b] Jéssica C. Gil [a,b], Nadezda V Tarakina,[c] Gelson T. S. T. Silva[a,b], José B. G. Filho,[d] Klaus Krambrock,[e] Markus Antonietti,[c] Cauê Ribeiro[b] and Ivo F. Teixeira* [a,c]

[a] Department of Chemistry, Federal University of São Carlos, 13565-905, São Carlos, SP, Brazil

[b] National Nanotechnology Laboratory for Agriculture, Brazilian Agriculture Research Corporation (Embrapa), XV de Novembro Street – 1452, São Carlos, Brazil

[c] Department of Colloid Chemistry, Max Planck Institute of Colloids and Interfaces, Am Mühlenberg 1, D-14476 Potsdam, Germany

[d] Department of Chemistry, Federal University of Minas Gerais (UFMG), 31270-901, Belo Horizonte, MG, Brazil

[e] Department of Physics, Federal University of Minas Gerais (UFMG), 31270-901, Belo Horizonte, MG, Brazil

Methods

Chemicals

All chemical reagents were purchased from Sigma-Aldrich except when is indicated. All the chemical reagents were of analytical grade and used without any further purification.

Na-PHI Synthesis

Na-PHI was synthesized using melamine (1 g) ground with NaCl (10 g). The reaction mixture was transferred to a porcelain crucible and heated up in a muffle furnace (Nabertherm) under constant nitrogen flow (1-5 L min^{-1}) to 600 °C with a heating rate of 2.3 °C min^{-1}, held at 600 °C for 4 h, and then allowed to cool down under natural cooling. The crude product was removed from the crucible, washed with deionized water (1 L), isolated by filtration, and then thoroughly washed with deionized water on the filter (1 L). The final product was dried in an oven at 60ºC for 8h under vacuum. The yield of Na-PHI synthesis is generally around 61%.

M-PHI Synthesis

The metal ions were introduced into the PHI structure by a cation exchange method, as reported in other studies[1, 2] (**Fig S1**). In each synthesis, Na-PHI (0.4 g) was suspended in water (20 mL) and, after 30 minutes, 2 mL of the metal chloride solution was added, the mixture was stirred for 1 hour. **Table S6** organizes the metal concentration inserted for each Cu-PHI catalyst, the same trend is applied to other metals (Co and Fe). After that, the M-PHI materials were separated by centrifugation in a 50 mL plastic tube (6.500 rpm, for 15 min), washed 5 times with deionized water (i.e. the materials were resuspended 5 times in water to extract all the remaining chloride precursor) and dried for 8h in an oven at 60 ºC.

Characterization

The X-ray powder diffraction patterns were recorded on Bruker D8 Advance diffractometer equipped with a scintillation counter detector with CuKα radiation ($\lambda = 0.15418$ nm) applying 2θ step size of 0.05° and counting time of 3 s per step. Steady-state UV–vis absorption spectra were acquired using Shimadzu UV 2600 in diffuse reflectance mode. Fourier transform infrared attenuated total reflectance (FTIR-ATR) spectra were recorded on a Varian1000 FT-IR spectrometer equipped with an attenuated total reflection unit with diamond, with a resolution of

4 cm^{-1}. Inductively coupled plasma-optical emission spectrometry (ICP-OES) was conducted using a Horiba Ultra 2 instrument equipped with photomultiplier tube detector.

For transmission (TEM) and scanning transmission electron microscopy (STEM) observations, a suspension of the sample in ethanol was sonicated for 10 min and then drop-casted to a Cu grid with a lacey carbon support and dried for 5 min. The (S)TEM study was performed using a double Cs corrected JEOL JEM-ARM200F (S)TEM operated at 80 kV and equipped with a cold-field emission gun and a high-angle silicon drift energy dispersive X-ray (EDX) detector (solid angle up to 0.98 steradians with a detection area of 100 mm^2). Annular dark-field scanning transmission electron microscopy (ADF - STEM) images were collected at a probe convergence semi-angle of 25 mrad. The “beam shower” procedure was performed for 30 min to reduce hydrocarbon contamination during subsequent imaging at high magnification.

Raman spectra were recorded using a confocal Raman microscope alpha300 (WITec, Germany) coupled with a laser excitation at wavelength of 785 nm. The laser beam of was focused through a Nikon 20 × microscope objective lens. The Raman spectra have been measured with an integration time of 10 s under excitation laser powers 60 mW, respectively. The spectra were acquired with a thermoelectrically cooled Andor CCD detector DU401A-BV placed behind the spectrometer UHTS 300 from WITec with a spectral resolution of 3 cm^{-1}. The Raman band of a silicon wafer at 520 cm^{-1} was used to calibrate the spectrometer. The experiments under the reaction condition were performed by dropping H_2O_2 on Cu-PHI, deposited over a glass microscope slide, the analysis was carried in the same way described above.

The Mott-Schottky measurements were performed in a Biologic MPG-2 system using a 3 electrode set up consisting of a Pt wire working as counter electrode, an Ag/AgCl as reference electrode F-doped tin oxide (FTO) glass coated with the material as working electrode. The working electrode was prepared on FTO glass that was cleaned by sonication in ethanol for 30 min and dried at 353 K. The boundary of FTO glass was protected using Scotch tape. The 3 mg sample was dispersed in 0.2 mL of water by sonication to get a slurry mixture with 20 μL of Nafion. The slurry was spread onto pretreated FTO glass. After air-drying, the Scotch tape was removed and the working electrode was further dried at 393 K for 2 h to improve adhesion.

X-ray photoelectron spectroscopy (XPS) measurements were performed on a ThermoScientific Escalab 250 Xi. A microfocused, monochromated Al Kα X-ray source (1486.68 eV) and a 400 μm spot size were used in the analysis. Samples were prepared using carbon tape. LiCl was added to each sample in order to calibrate the binding energies towards Li. ThermoScientific Avantage software was used to analyze the resulting spectra.

Time-resolved fluorescence measurements were performed by using a single photon counting setup (TCSPC) with a Becker&Hickl PML-spectrometer (modified Oriel MS-125) with a laser repetition rate of 2 MHz. The detector comprises a Becker&Hickl PML-16-C-1 (modified Hamamatsu) multi-alkaline photomultiplier. The excitation wavelength was 405 nm. The excitation was carried out using a pulsed laser diode at ~30 nJ/cm² (LDH-P-C405, PicoQuant GmbH). The emission was recorded in the range of 460-600 nm, while blocking the secondary detection of the excitation pulses with a 450 nm cut-off-filter. Raw decay data presented as logarithm of photon counts versus time were analyzed with data analysis software of PicoQuant GmbH (Germany)

Photocatalytic Tests

Methane photo-oxidation tests was carried out in a quartz tube (140 mL) illuminated with 6 visible light lamps (15 W) (**Fig S15**). The reaction temperature was maintained at 25ºC using a thermostatic bath. In each test, 50 mg of photocatalyst was added to a hydrogen peroxide solution (0.8 mM) in deionized water. In order to saturate the reactor, CH_4 (99.9%) was bubbled into the suspension with a constant flow for 15 minutes. The production of CO_2 and CO was analyzed at the end of the reaction (4 h) in a gas chromatograph (Thermo CP-3800) equipped with a flame ionization detector (FID) and a thermal conductivity detector (TCD) with a packed HayeSep N column (0.5 m x 1.8”) and a 13X molecular sieve column (1.5 m x 1.8”). Argon was used as the carrier gas, and the methanizer temperature was 350 °C.

Liquid products were quantified by ^{1}H nuclear magnetic resonance (NMR) (600 MHz, Ascend™ 600 Bruker) at 25 °C. For each test, 540 µL of the sample was mixed with 60 µL of D_2O solution containing 5.0 mM dimethyl sulfoxide (DMSO) as a standard and 0.21 mM $TSPd_4$ as a reference. A WET procedure suppressed the water peak. Nuclear magnetic resonance data were processed using the MestReNova software. Representative ^{1}H NMR spectra used to determine and calculate the concentration of liquid products are shown in **Fig S16**.

The quantification of liquid products by NMR ^{1}H for all compounds follows the equation described below:

$$\mu\text{mols} = \frac{\text{Compound Area x 6 (number of H of DMSO) x 5 (Concentration of DMSO in } \mu\text{mols)}}{\text{DMSO Area x Number of H of the compound}}$$

To confirm the quantification of NMR experiments, methanol and ethanol were also quantified by GC-FID (using a DB-WAX column and He as carrier gas). For each test, 150 µL of reaction sample was mixed with 50 µL of a 1-Octanol solution (1.5 mM) in high purity CH_3CN (99.99%). To ensure that methanol was only present in the reaction sample, blanks with deionized water and the external standard were injected. The chromatogram of a methanol and ethanol solution is exhibit in **Fig S17**. Calibration curve of methanol using GC-FID is shown at **Fig S18**.

The concentration of liquid formaldehyde (HCHO) was quantified by the colorimetric method described elsewhere.[3] An aqueous solution (100 mL) was prepared by dissolving 15 g of ammonium acetate, 0.3 mL of acetic acid, and 0.2 mL of pentane-2,4-dione. Then, 0.5 mL of reaction liquid product was mixed with 2.0 mL of water and 0.5 mL of reagent solution. The mixed solution was maintained at 35 °C and measured by UV−Vis absorption spectroscopy at 412 nm. The concentration of HCHO in the liquid product was determined by the calibration curve (**Fig S21**).

Methane conversion was calculated based on the sum of methane in liquid (dissolved in water) and gaseous phases. Liquid methane was extracted from Duan and Mao's study[4], which predicts that solubility of methane in pure H_2O is 0.00126 $mol.kg^{-1}$. Since 100 mL of water was used at methane oxidation reactions, we can assume that 126 µmols of CH_4 is present in liquid phase. Methane in gaseous phase was calculated based on STP conditions, i.e. 1 mole of gas at 25 L. Therefore, 1600 µmols of CH_4 was considered in 40 mL of headspace. Methane conversion was calculated as follows:

$$CH_4 \text{ Conversion} = \frac{\text{Sum of all gaseous and liquid products (µmols)}}{1600+126 \text{ µmols}} \text{ x } 100\%$$

EPR measurements

EPR measurements allied to spin trapping methodology were conducted using 5,5-dimethyl-1-pyrroline n-oxide (DMPO, CAS 3317-61-1, 96%, Oakwood, EUA) and N-tert-Butyl-α-phenylnitrone (PBN, CAS 3376-24-7, 98%, TCI America, Japão). For the measurements a Magnettech Mini Scope MS400 EPR X-Band spectrometer were used operating with the following configurations: 10 mW microwave power, 100 kHz modulation field with 0.2 mT amplitude, 337 mT centered field, 60 s scan time and 4096 integration points. Low temperature measurements were performed on another MiniScope 400 EPR spectrometer modified by an ESR 900 cryosystem (Oxford Instruments, United Kingdom) using a liquid helium flow. The temperature was controlled by MercuryIC (Oxford Instruments, United Kingdom).

For the spin trapping experiments with DMPO, 20 mg of this spin trap were solubilized in 1 mL of solvent: (i) deionized water to detect $^{\bullet}OH$ radicals or (ii) acetonitrile saturated with oxygen to observe $O_2^{\bullet -}$ radicals. For the spin trapping tests involving PBN, 25 mg of this compound was solubilized in 1 mL of a 1:1 solution (ethanol/ water) to evaluate the kinetics of hydroxyl radicals (indirectly) or in methanol to evaluate the formation of alcohol radicals. In these solutions, 5 mg of photocatalyst was suspended, 6 µL of H_2O_2 (30 % V/V) were added and the systems was illuminated with a white LED lamp with irradiance of 16 mW.cm^{-2}. Aliquots were removed with the aid of a glass capillary (~ 50 µL) and placed in a quartz tube (Wilmad Labglass, United States,) which was then inserted into the cavity of the EPR spectrometer. The adducts were simulated using Easyspin[5].

SUPPLEMENTARY TABLES

Table S1 Vibrational modes and corresponding Raman shifts for M-PHIs materials.

Raman Shift (cm^{-1})	Correspondence
200-300	Metal-N
469	In-plane Ring Torsion
657	Vibration (C-N)
733	Heptazine Breathing Mode
799	Vibration (C-N)
936-1020	Vibration (N-C=N) Out-of-plane Bending (C-(N)$_3$)
1104	Vibration (C-N)
1162	Vibration (N-C=N) Bending (N-H)
1234 e 1273	Bending (N-C=N)

Table S2 Methane oxidation results from literature.

				Production (μmol.g^{-1})		
Catalyst	**Oxidant**	**Pressure**	**Time (h)**	**CH_3OH**	**Total Oxygenates**	**Reference**
Cu-PHI 0.5%	H_2O_2 (80 μmol)	CH_4 (1 bar)	4	2900	3760	This Work
FeO_x/TiO_2 0.33 wt%	H_2O_2 (80 μmol)	CH_4 (1 bar)	3	1056	1156	6
Cu-0.5/PCN	H_2O	CH_4/N_2 (1:9) (1 bar)	1	24.5	130.5	7
Au0.30/ZnO	O_2 (5 bar)	CH_4 (15 bar)	2	1996	2403	8
RCN-5	O_2 (1 bar)	CH_4 (20 bar)	3	75	925	9
1.98%FeOOH/m-WO_3	H_2O_2 (1.5 mM)	CH_4/N_2 (1:9) (1 bar)	4	844.8	844.8	10
Au1/BP	O_2 (3 bar)	CH_4 (30 bar)	2	113.5	113.5	11
RhB/TiO_2	H_2O_2 (50 μL)	CH_4 (20 bar)	4	572	572	12
1.0% Cu-SAs/C_3N_4*	H_2O_2 (5 mL)	CH_4 (30 bar)	5	397	3500	13
2.7% FeN_4/GN*	H_2O_2 (5 mL)	CH_4 (20 bar)	10	-	2300	14

* Catalytic systems (without light).

Table S3 Methane photo-oxidation results of the catalysts synthesized in this work. Productions below 20 µmol.g^{-1} are considered negligible.

	Production (µmol.g^{-1})			
Photocatalyst	**Methanol**	**C2/C3 Products***	**CO_2**	**Conversion (%)**
Na-PHI	-	-	-	-
Co-PHI 10%	180	-	-	0.5
Fe-PHI 10%	260	28	380	1.9
Cu-PHI 10%	670	60	-	2.1
Cu-PHI 4%	1450	550	-	5.8
Cu-PHI 1%	2160	810	-	8.6
Cu-PHI 0,5%	2900	1160	-	11.7
Cu-PHI 0,1%	220	80	-	0.9

*C3 Products are only observed with Cu-PHI 0.5% and 1%, generating isopropanol and acetone as liquid products. HCHO was observed with Cu-PHI 0.5%, 1% and 4%.

Table S4 Metal loading measured by ICP-OES for the catalysts.

Photocatalyst	Metal Loading (m/m %)
Co-PHI 10%	9.8
Fe-PHI 10%	9.6
Cu-PHI 10%	10.4
Cu-PHI 4%	4.4
Cu-PHI 1%	1.1
Cu-PHI 0.5%	0.48
Cu-PHI 0.1%	0.09
Cu-PHI 0.5% (After 1 Cycle)	0.48
Cu-PHI 0.5% (After 3 Cycles)	0.46

Table S5 Time-resolved photoluminescence fluorescence lifetimes for the catalysts and with the addition of hydrogen peroxide.

Photocatalyst	**τQ_{avar} (ns)**
Co-PHI 0.1%	0.52
Fe-PHI 0.5%	0.27
Cu-PHI 0.5%	0.37
Na-PHI	0.37
Cu-PHI 0.5% + H_2O_2	0.21
Co-PHI 0.5% + H_2O_2	0.77
Fe-PHI 0.5% + H_2O_2	0.75
Na-PHI 0.5% + H_2O_2	0.78

Table S6 Quantities of copper chloride added to Na-PHI suspension during the cation exchange procedure and its respective yields.

Photocatalyst	**Amount of $CuCl_2.6H_2O$ (mmol)**	**Yield (%)**
Cu-PHI 0.1%	0.0064	95
Cu-PHI 0.5%	0.032	91
Cu-PHI 1 %	0.064	92
Cu-PHI 4 %	0.30	89
Cu-PHI 10 %	1.00	65

FIGURES

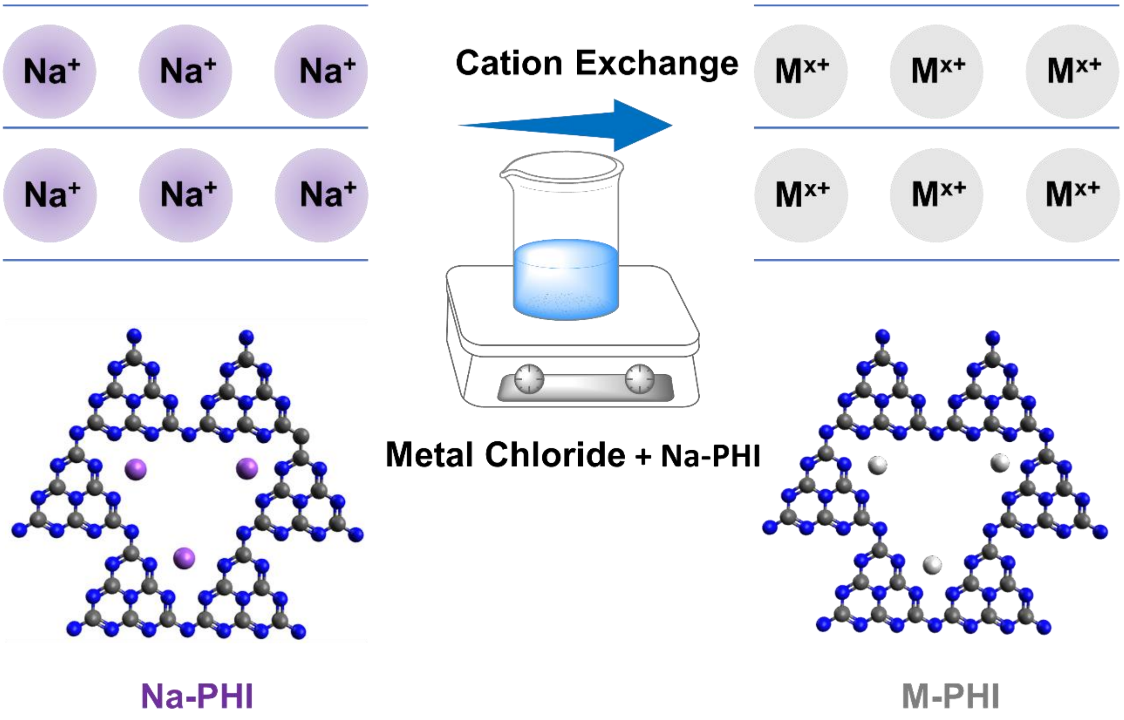

Fig. S1 Schematization of cation exchange method to coordinated transition metal in PHI structure.

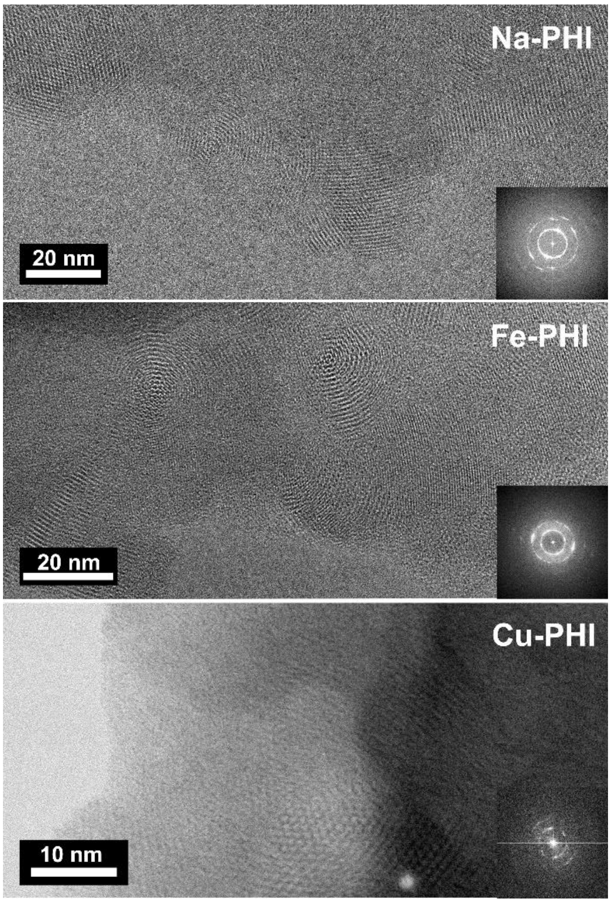

Fig S2 HR-TEM images of Na-PHI and Fe-PHI samples, as well as BF-STEM image of Cu-PHI. Insets show fast Fourier transforms obtained from presented area.

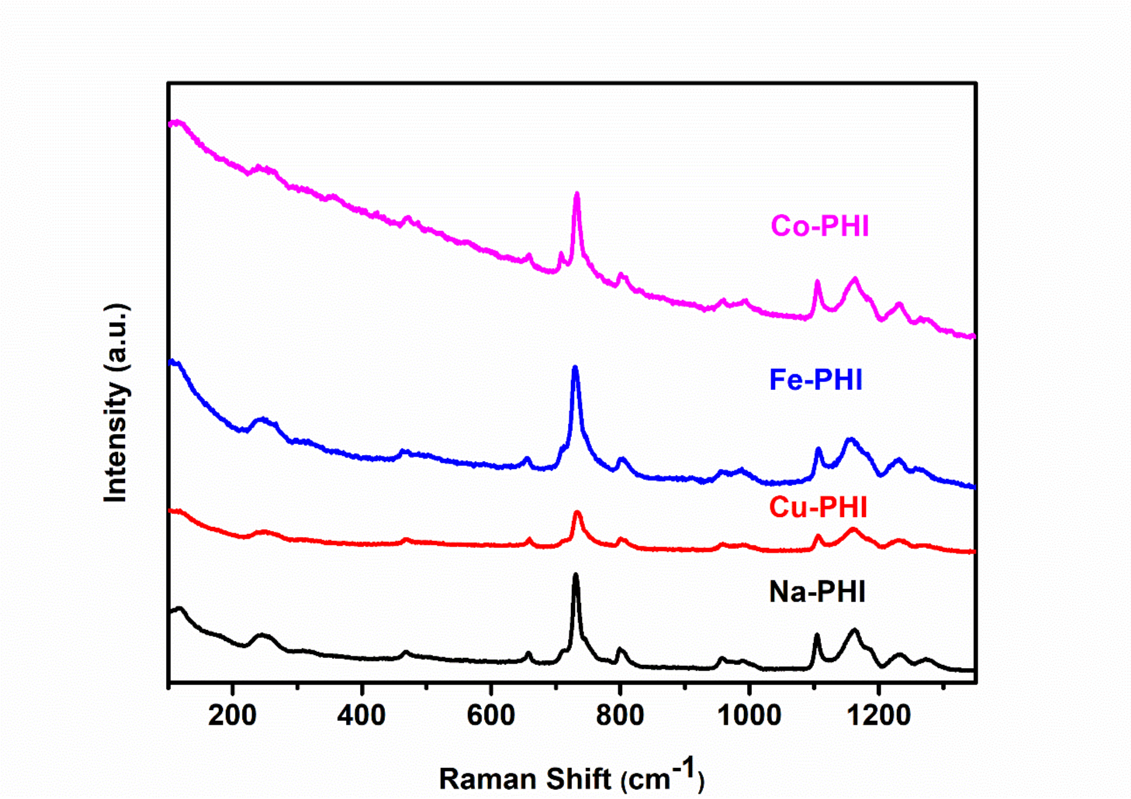

Fig. S3 Raman spectra of M-PHIs.

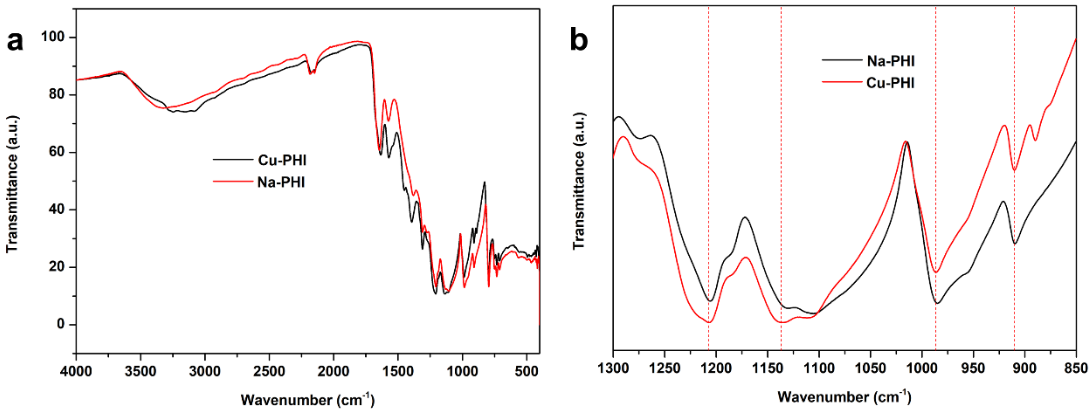

Fig S4 FTIR spectra for Cu-PHI and Na-PHI showing slighter shifts in wavenumbers, indicating coordination of metal atoms in PHI structure.

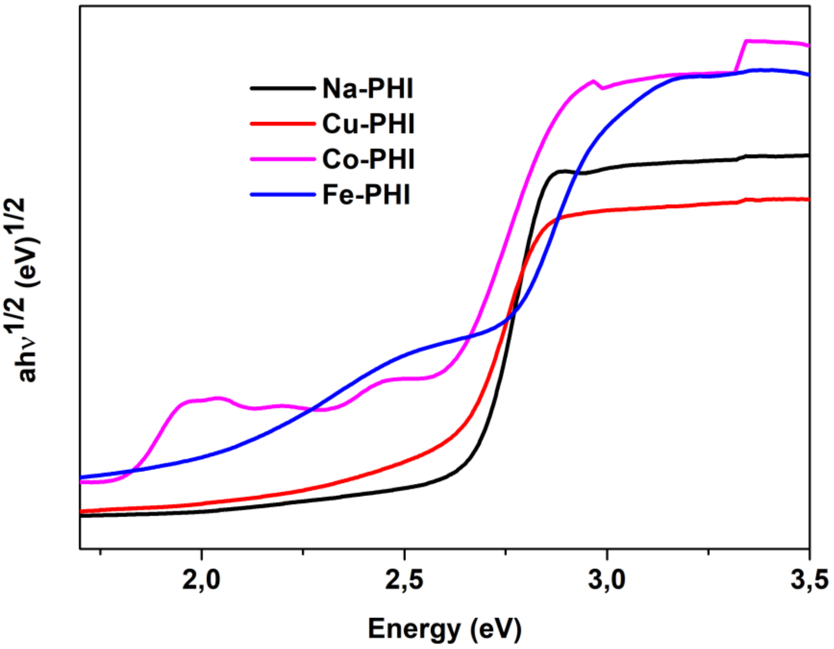

Fig S5 UV-Vis diffuse reflectance spectra for M-PHI samples. Co-PHI and Fe-PHI shows intragap absorptions, while Cu-PHI shows similar trend of Na-PHI. Band gap energy was evaluated by major absorption edge for each material. The energy values are 2.7 eV for Na, Fe, and Cu-PHI, and 2.5 eV for Co-PHI.

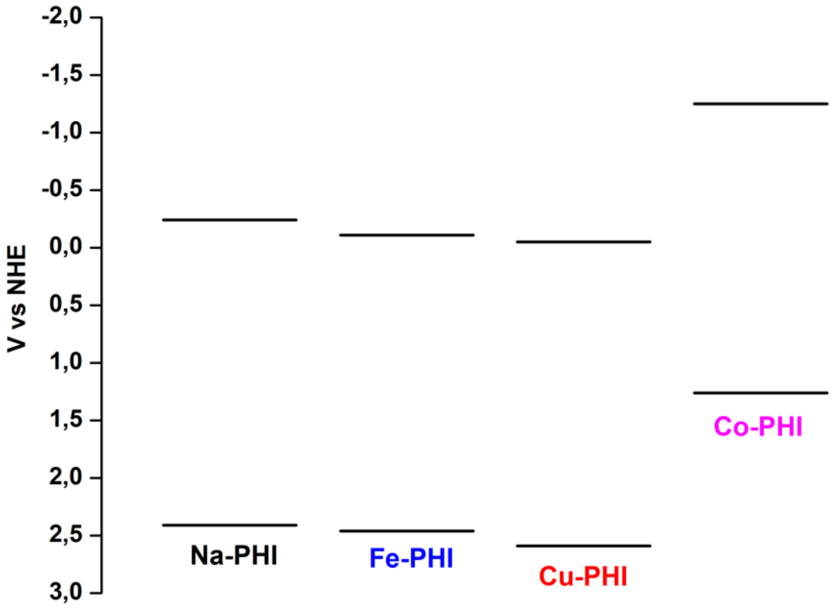

Fig. S6 Band potential diagram of Na, Fe, Cu and Co-PHI.

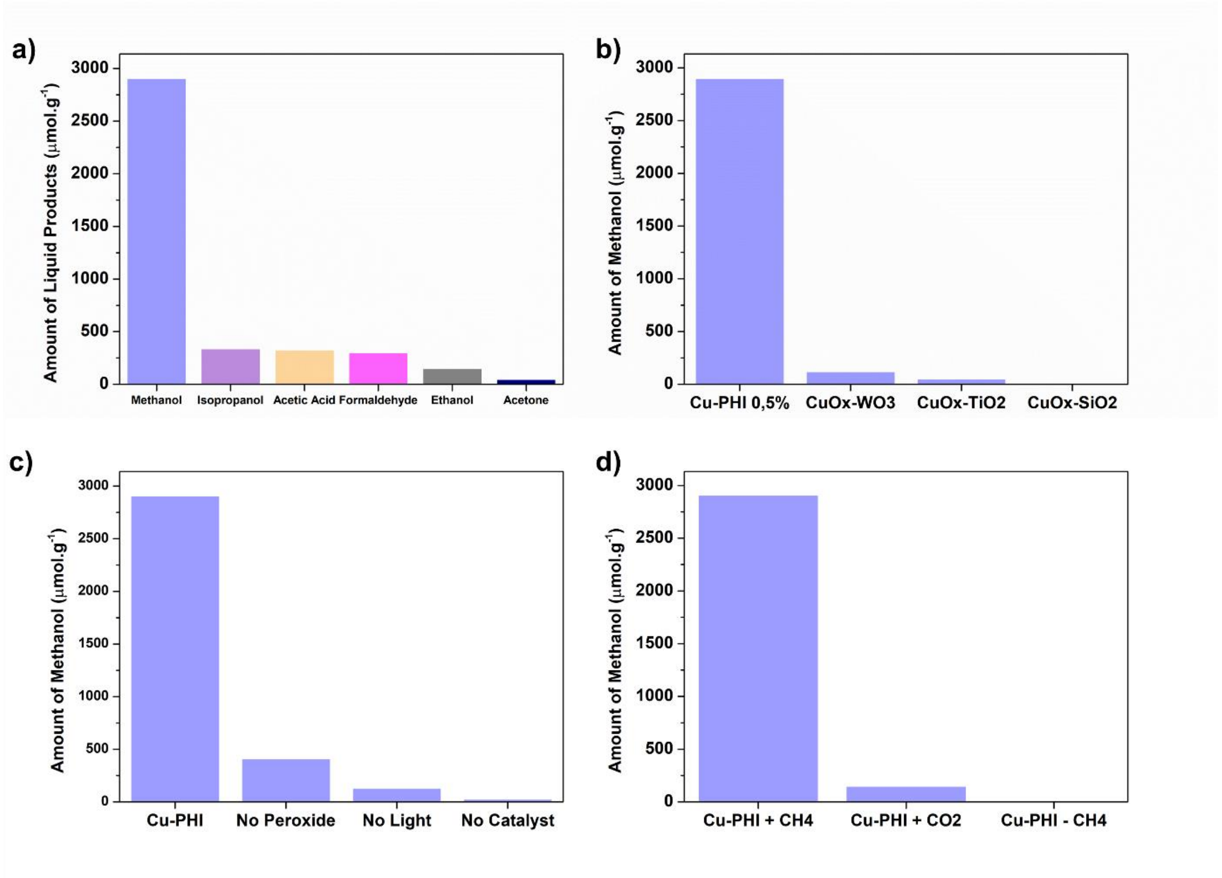

Fig. S7 (a) Distribution of liquid products for methane photo-oxidation reaction with Cu-PHI 0.5%; (b) Amount of methanol with different supports loaded with 0.5% of Cu; (c) Amount of methanol with Cu-PHI 0.5% under the absence of one of the initial conditions; (d) Amount of methanol with Cu-PHI 0.5% with CH_4, CO_2, and without CH_4. Reaction conditions: 50 mg of photocatalyst, 100 mL deionized H_2O, 80 µmol of H_2O_2, visible light, 1 bar CH_4 (1 bar CO_2 for Cu-PHI + CO_2 in Fig S7d and 1 bar N_2 for Cu-PHI – CH_4 in Fig S7d), 25 °C, 4h of reaction.

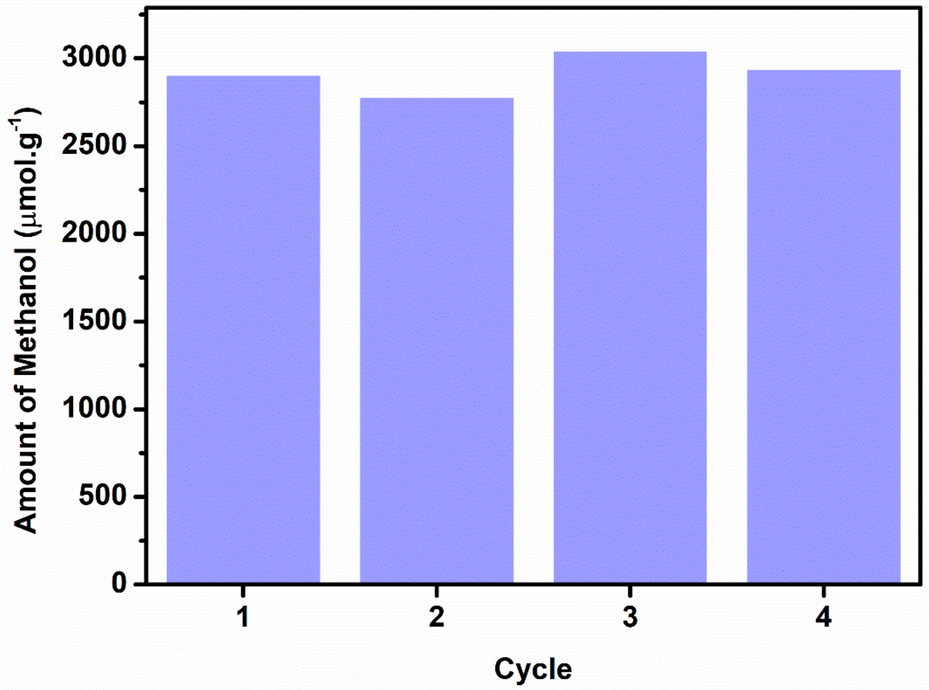

Fig S8 Recycling tests of Cu-PHI 0.5%. Reaction conditions: 50 mg of photocatalyst, 100 mL deionized H_2O, 80 µmol of H_2O_2, visible light, 1 bar CH_4, 25 °C, 4h of reaction.

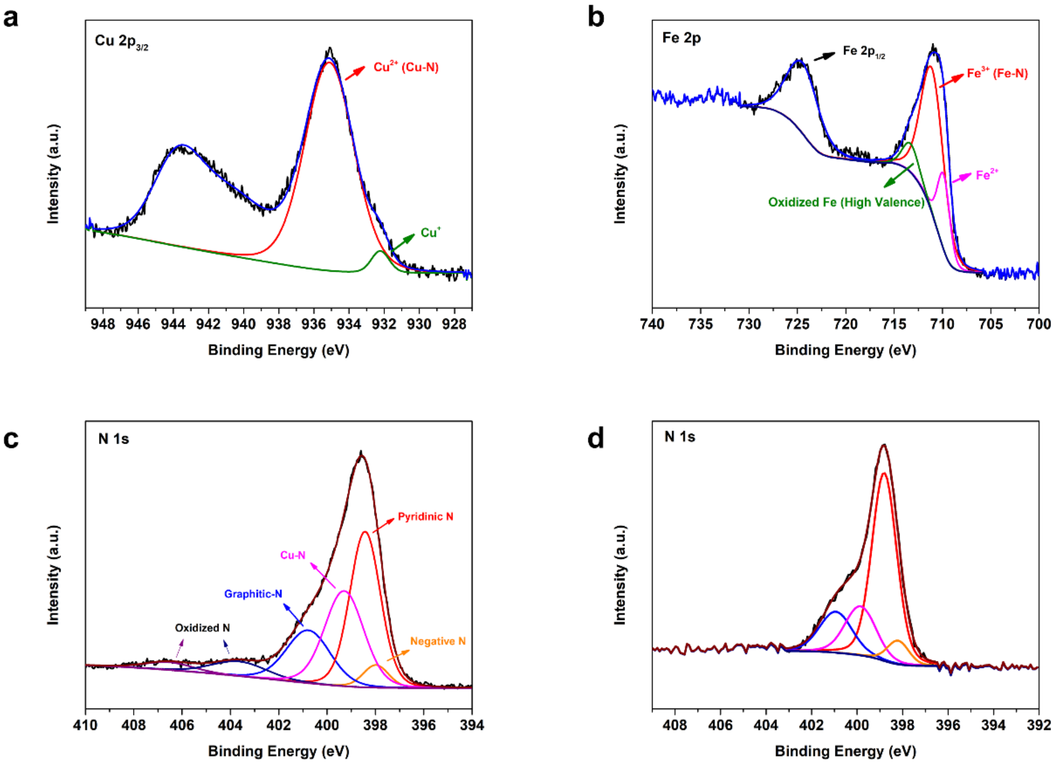

Fig. S9 High-resolution XPS spectra of Cu $2p_{3/2}$ **(a)** and N 1s **(c)** of Cu-PHI, and Fe 2p **(b)** and N 1s **(d)** of Fe-PHI.

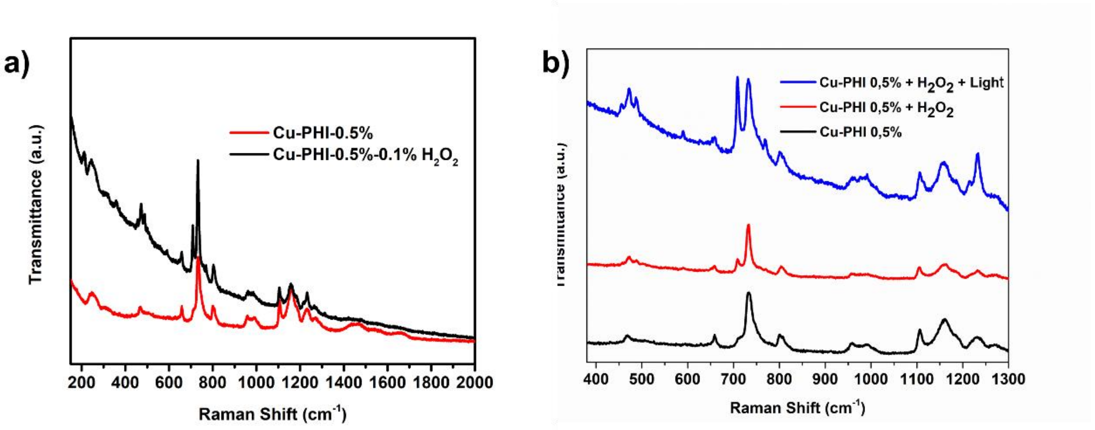

Fig. S10 Full Raman spectra of Cu-PHI 0.5% with H_2O_2 **(a)**, and H_2O_2 with light **(b).**

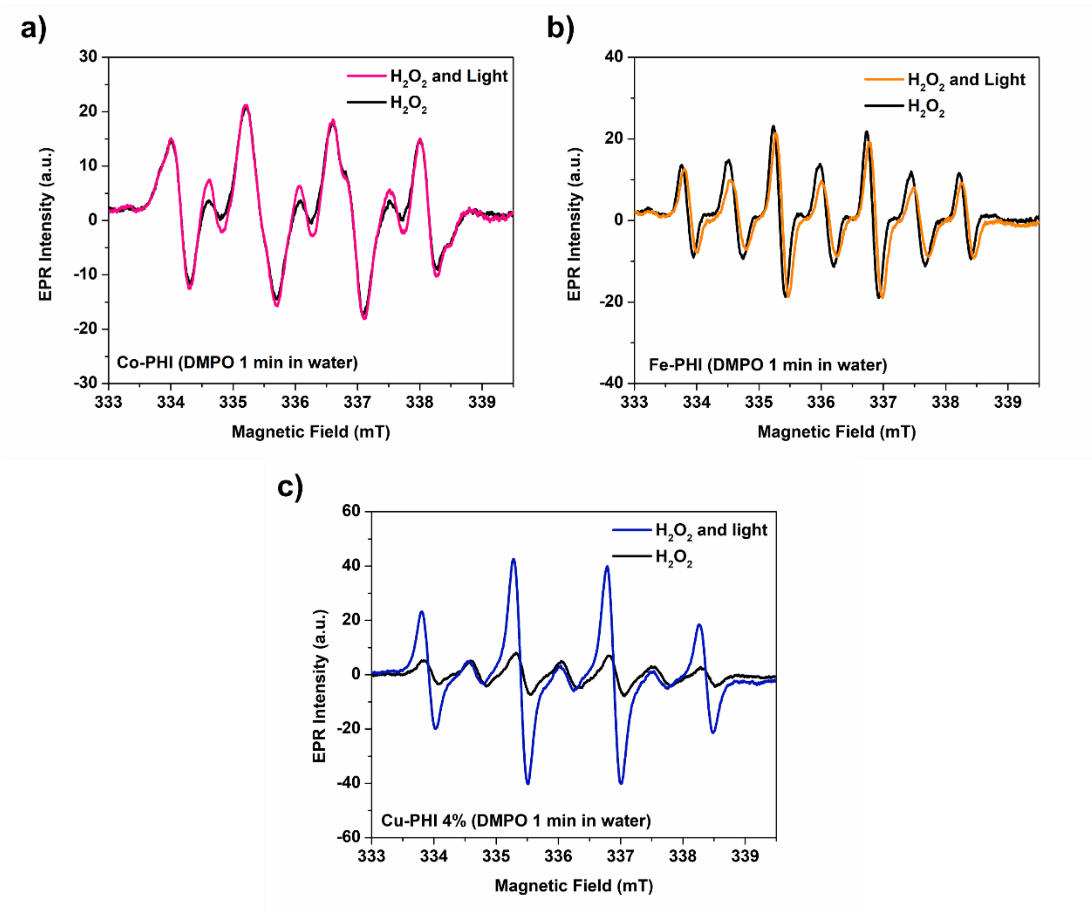

Fig S11 EPR spectra of DMPO adducts in water with H_2O_2 in the presence and absence of visible light radiation (recorded 1 min after the H_2O_2 addition) for samples (a) Co-PHI, (b) Fe-PHI and (c) Cu-PHI 4%.

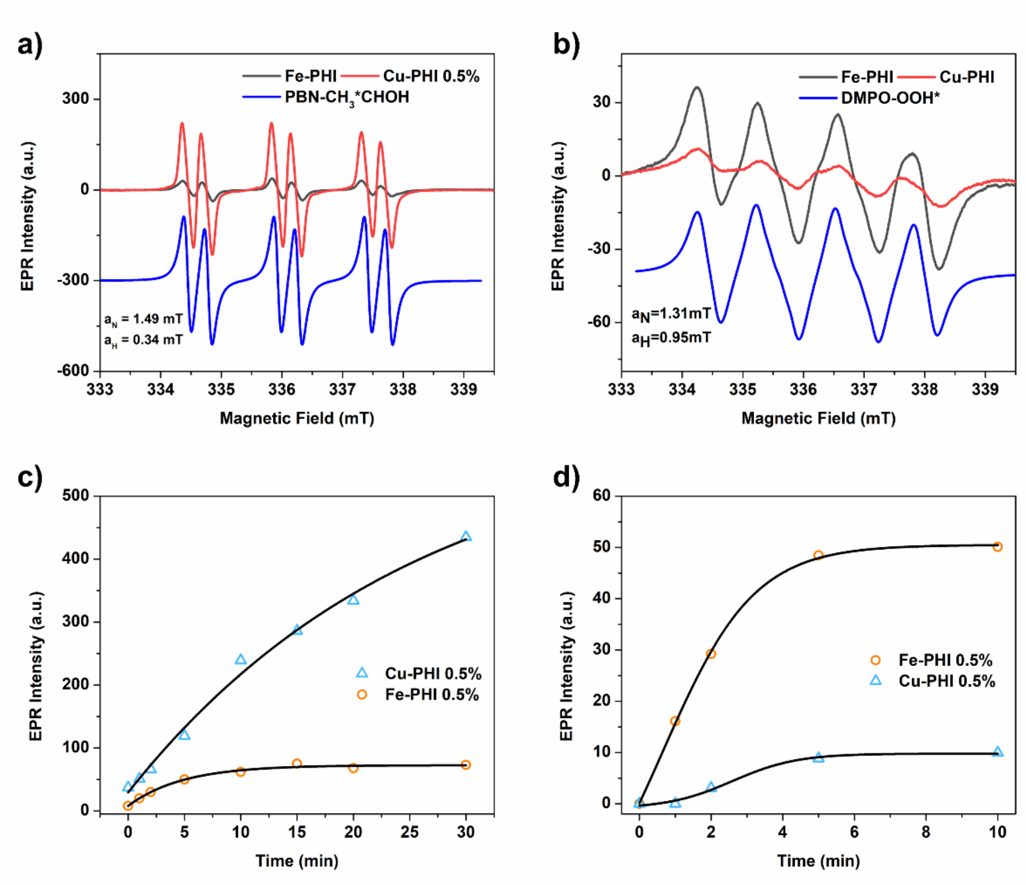

Fig S12 EPR spectra of (a) PBN in water/ethanol mixture and (b) DMPO in acetonitrile spin adducts and kinetic profile of their adducts (c) and (d), respectively. These results were obtained for Fe-PHI and Cu-PHI 0.5% samples through white LED illumination.

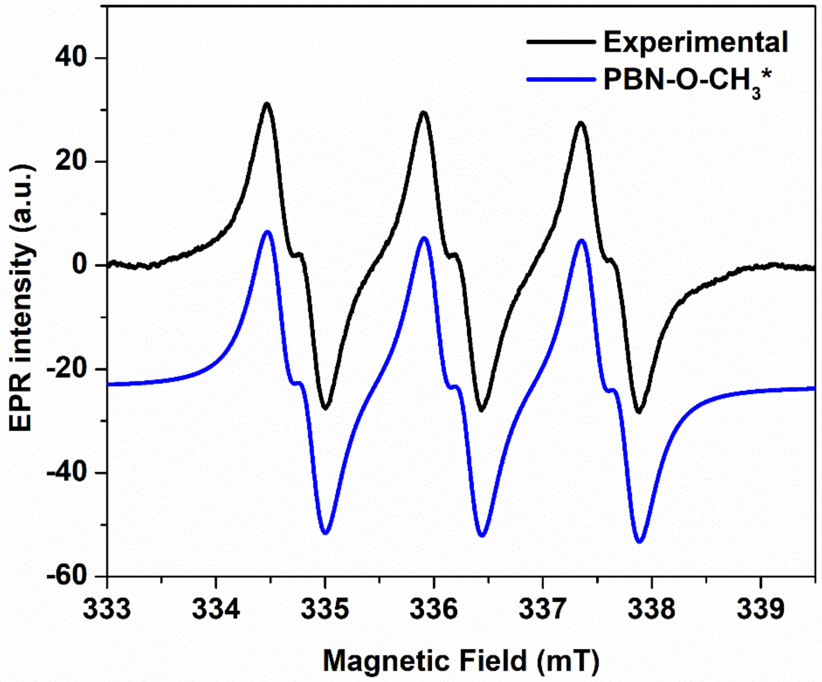

Fig S13 EPR spectra Calculated (blue) and experimental (black) EPR spectra of the PBN-methoxy adduct.

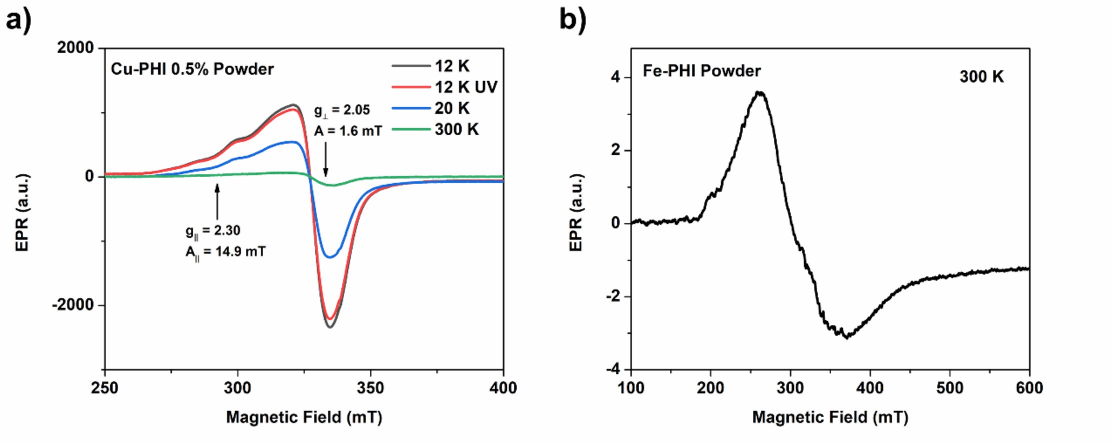

Fig S14 EPR powder spectra of (a) Cu-PHI 0.5% at different temperatures and (b) the Fe-PHI powder spectrum measured at room temperature.

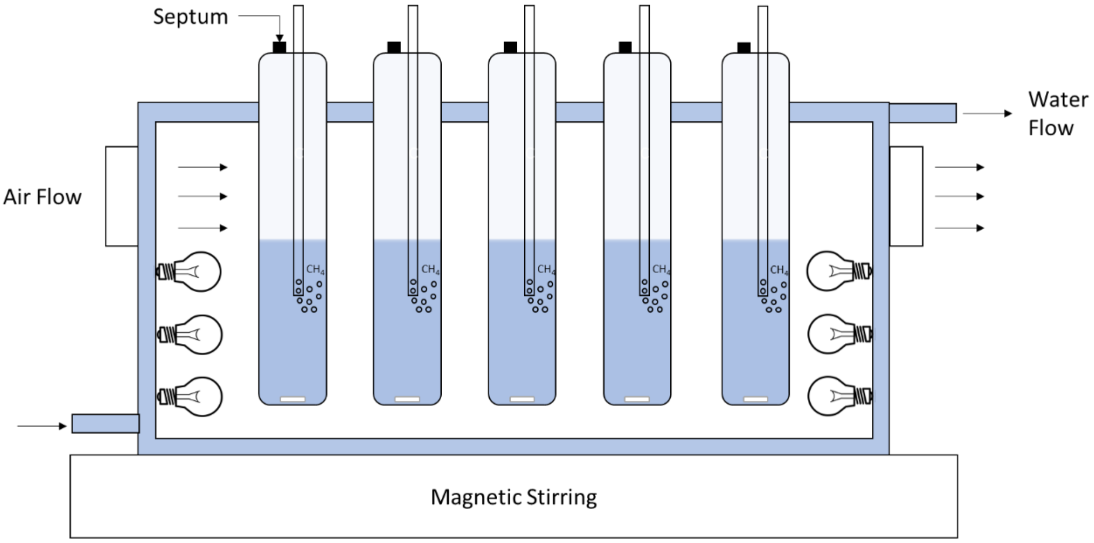

Fig S15 Schematic representation of photocatalytic system for methane oxidation reactions.

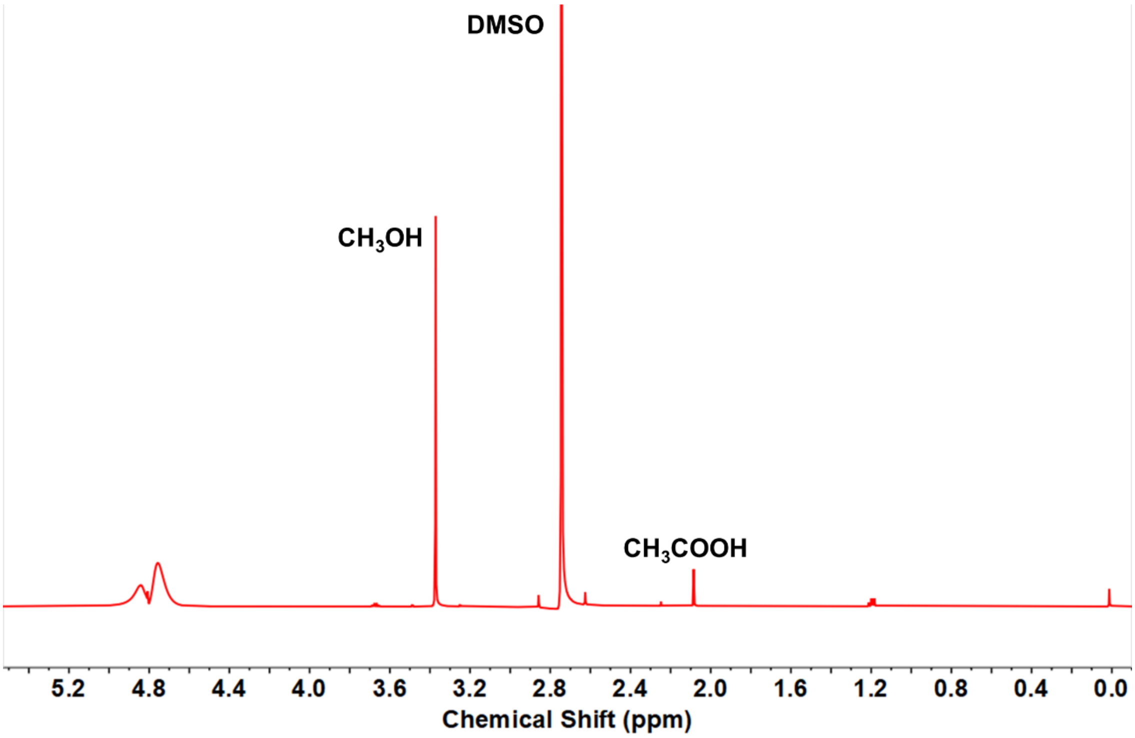

Fig S16 NMR ^{1}H of methane oxidation reactions products with Cu-PHI 0.5%.

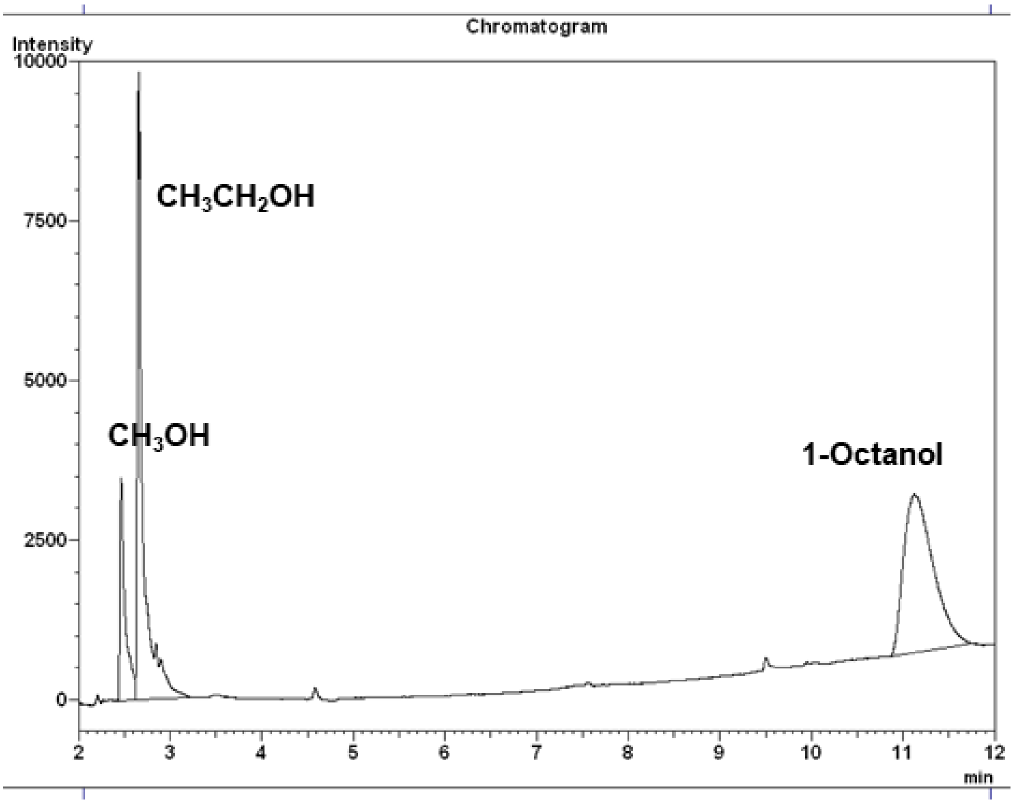

Fig S17 Chromatogram of equimolar quantities of methanol and ethanol with 1-Octanol (1,5 mM) as external standard.

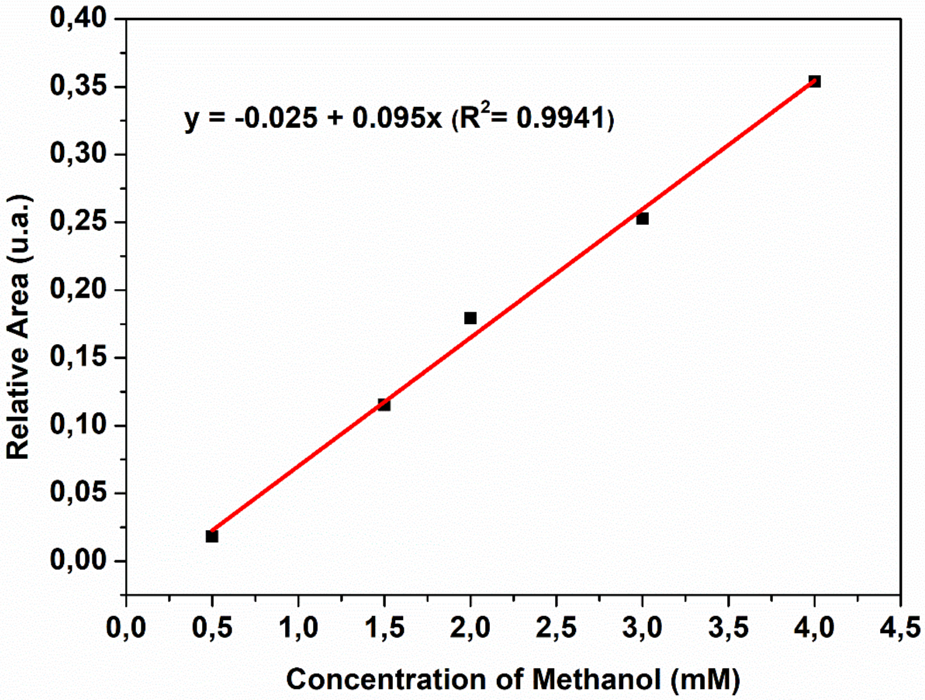

Fig S18 Calibration curve of methanol calculated by GC-FID using 1-Octanol as external standard.

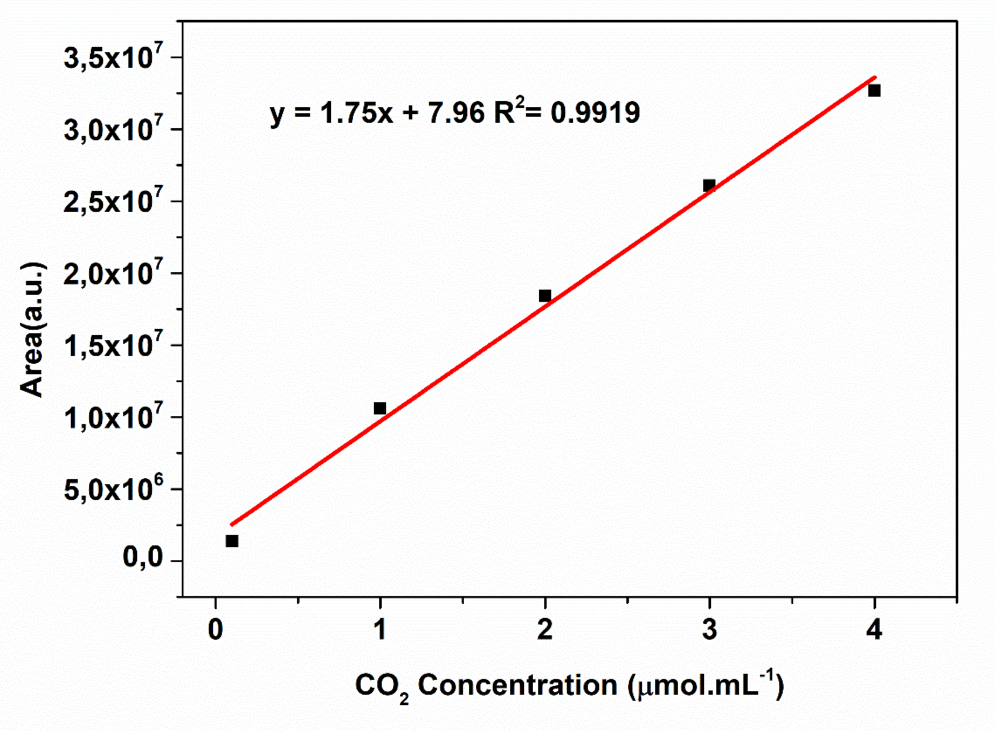

Fig S19 Calibration curve of CO_2 calculated by GC-TCD.

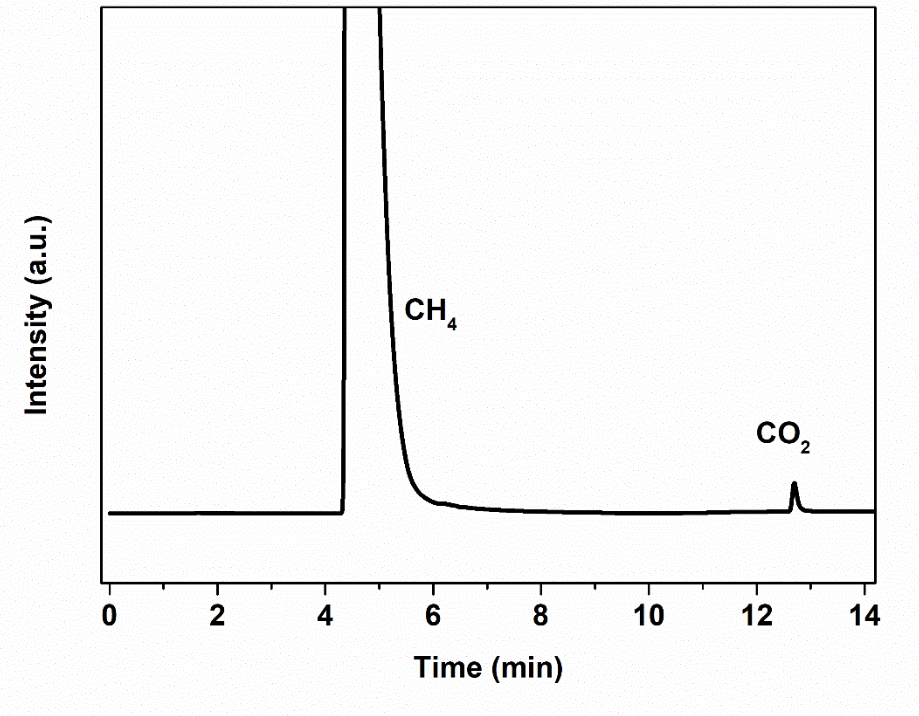

Fig S20 Chromatogram of GC-TCD showing peaks for Fe-PHI 10% methane photooxidation reaction. For Cu-PHI reactions, CO_2 does not appear. Other compounds could be identified, such as H_2 (1.5 min), O_2 (2.5 min) and CO (2.7 min).

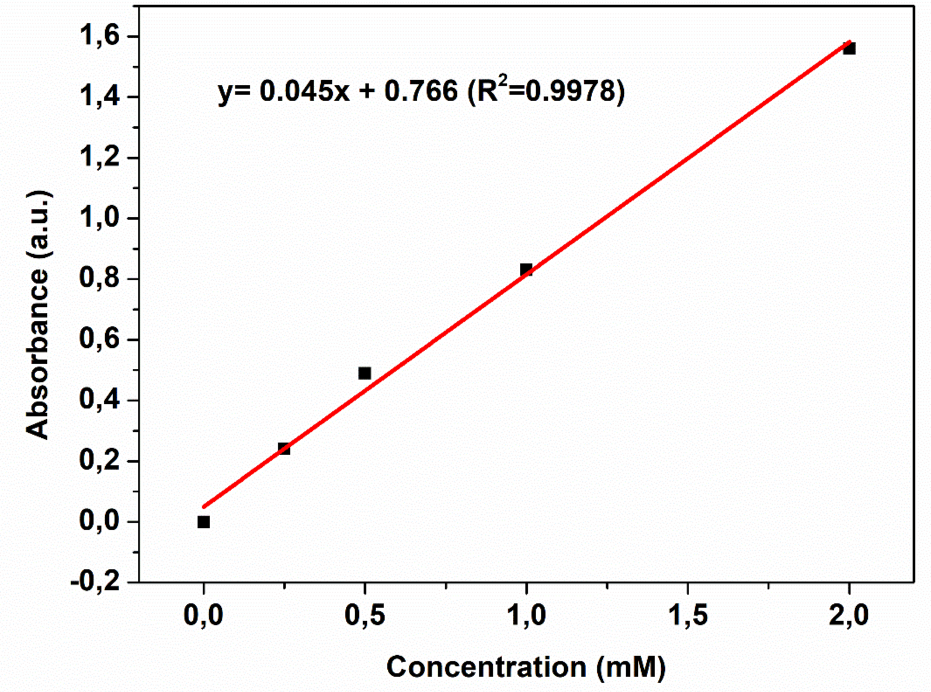

Fig S21 Calibration curve for formaldehyde quantification by colorimetric method.

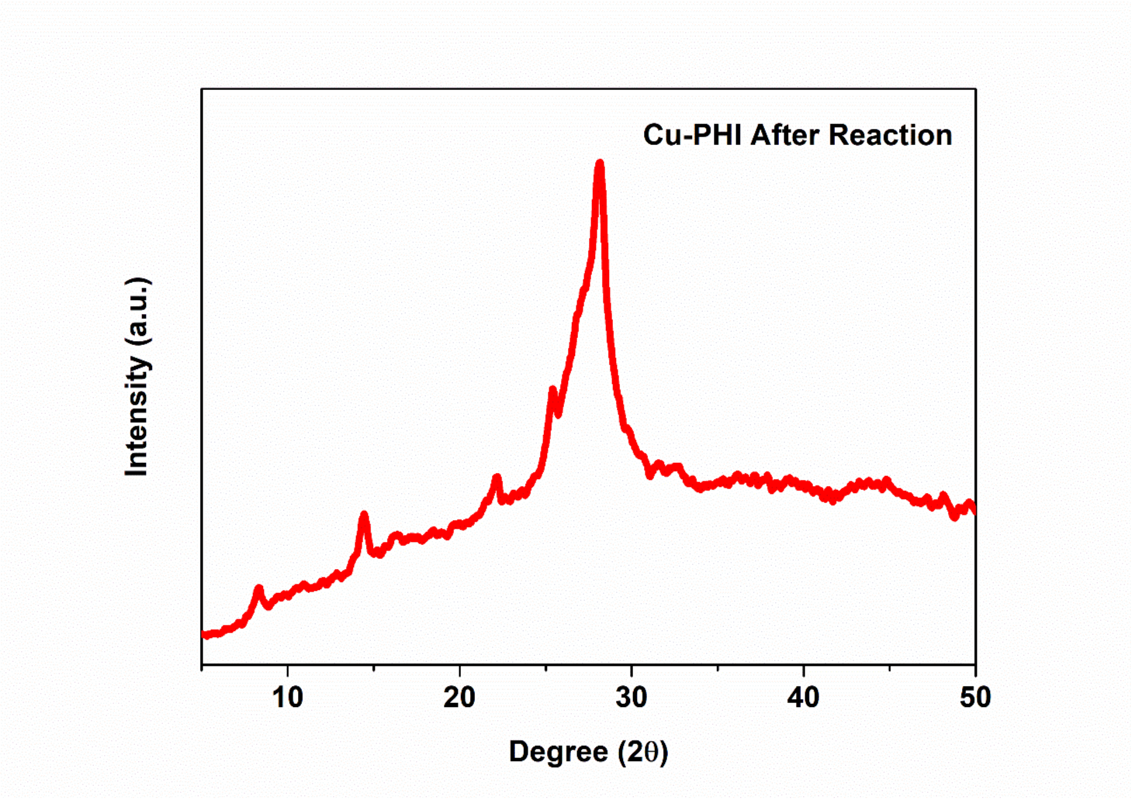

Fig S22 XRD of Cu-PHI 0.5% after reaction. The strong broad peak between 20-30° indicated that 2D distance is distorted after the break of symmetry promoted by reaction conditions (see Raman). However, the structural integrity of the Cu-PHI is mostly preserved.

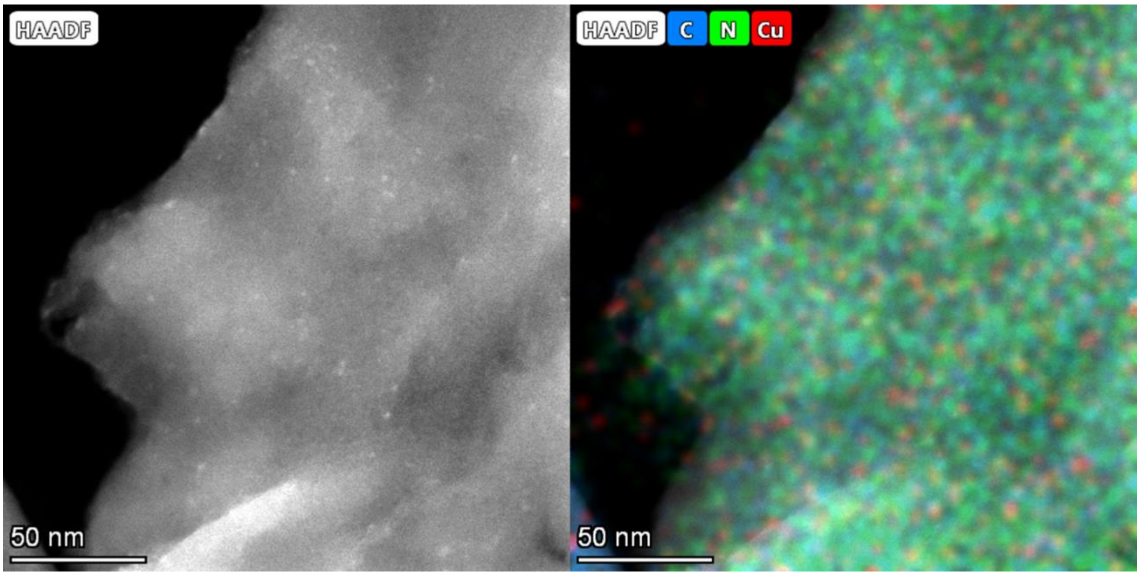

Fig S23 EDX mapping of Cu-PHI 0.5% using HAADF-STEM.

REFERENCES

1. F. M. Colombari, M. A. R. da Silva, M. Homsi, B. R. L. Souza, M. Araujo, J. L. Francisco, G. T. S. T. Silva, I. F. Silva, A. F. de Moura and I. F. Teixeira, *Faraday Discussions*, 2020.
2. M. A. da Silva, I. F. Silva, Q. Xue, B. T. Lo, N. V. Tarakina, B. N. Nunes, P. Adler, S. K. Sahoo, D. W. Bahnemann and N. López-Salas, *Applied Catalysis B: Environmental*, 2022, **304**, 120965.
3. H. Song, X. Meng, S. Wang, W. Zhou, X. Wang, T. Kako and J. Ye, *Journal of the American Chemical Society*, 2019, **141**, 20507-20515.
4. Z. Duan and S. Mao, *Geochimica et Cosmochimica Acta*, 2006, **70**, 3369-3386.
5. S. Stoll and A. Schweiger, *Journal of magnetic resonance*, 2006, **178**, 42-55.
6. J. Xie, R. Jin, A. Li, Y. Bi, Q. Ruan, Y. Deng, Y. Zhang, S. Yao, G. Sankar and D. Ma, *Nature Catalysis*, 2018, **1**, 889-896.
7. Y. Zhou, L. Zhang and W. Wang, *Nature communications*, 2019, **10**, 1-8.
8. W. Zhou, X. Qiu, Y. Jiang, Y. Fan, S. Wei, D. Han, L. Niu and Z. Tang, *Journal of Materials Chemistry A*, 2020, **8**, 13277-13284.
9. Z. Yang, Q. Zhang, L. Ren, X. Chen, D. Wang, L. Liu and J. Ye, *Chemical Communications*, 2021, **57**, 871-874.
10. J. Yang, J. Hao, J. Wei, J. Dai and Y. Li, *Fuel*, 2020, **266**, 117104.
11. L. Luo, J. Luo, H. Li, F. Ren, Y. Zhang, A. Liu, W.-X. Li and J. Zeng, *Nature communications*, 2021, **12**, 1-10.
12. X. Wu, Y. Zeng, H. Liu, J. Zhao, T. Zhang and S. L. Wang, *Nano Research*, 2021, **14**, 4584-4590.
13. B. Wu, R. Yang, L. Shi, T. Lin, X. Yu, M. Huang, K. Gong, F. Sun, Z. Jiang and S. Li, *Chemical Communications*, 2020, **56**, 14677-14680.
14. X. Cui, H. Li, Y. Wang, Y. Hu, L. Hua, H. Li, X. Han, Q. Liu, F. Yang and L. He, *Chem*, 2018, **4**, 1902-1910.